Available online at www.sciencedirect.com

ScienceDirect

Procedia CIRP 75 (2018) 81–86

www.elsevier.com/locate/procedia

15th CIRP Conference on Computer Aided Tolerancing – CIRP CAT 2018

Prediction and visualization of achievable orientation tolerances for additive manufacturing

Hannah Budinoff[a,*], Sara McMains[a]

[a]*Department of Mechanical Engineering, University of California, Berkeley, CA 94720, United States*

[*] Corresponding author. *E-mail address:* hdb@berkeley.edu

Abstract

In additive manufacturing, process parameters can have a large influence on the quality of the produced part, making it difficult to understand what tolerances are actually achievable. We present a system that can rapidly analyze part geometry and predict parallelism, perpendicularity, and angularity geometric deviations for planar surfaces, based on layer thickness and build direction. Our system can analyze multiple distinct features and their corresponding tolerances and datums to identify build directions where all specified tolerances can be achieved. This tool can be used to select an optimal build direction and to analyze whether specified tolerances are manufacturable using additive manufacturing.

Peer-review under responsibility of the Scientific Committee of the 15th CIRP Conference on Computer Aided Tolerancing - CIRP CAT 2018.

Keywords: Additive manufacturing; tolerancing; geometric deviations

1. Introduction

As additive manufacturing (AM) becomes more accepted as a viable manufacturing option for producing commercial products, there is a growing need to consider how to efficiently design and manufacture parts with acceptable geometric accuracy. AM processes build parts layer by layer, creating stair-step deviations on part surfaces. The geometric deviation due to the layers is a function of layer thickness and build direction [1]. Although process factors such as shrinkage can also impact geometric deviations, this work focuses on predicting geometric deviations due to the layered approximation.

In this paper, we describe a design-for-manufacturing tool that provides a designer with a real-time estimate of whether specified geometric tolerances are mutually achievable for a particular AM process, based on mathematical analysis of error as a function of build direction. Build direction also influences manufacturing time and total volume of material used, which are important manufacturing cost considerations. The design and tolerance allocation process can be improved when designers leverage knowledge about the connections between AM process parameters and resulting geometric deviations. Designers and manufacturers can also use this knowledge to specify a build direction that minimizes geometric error on key features of their part. Our main contributions include:

- Analysis of how the layered approximation of the datum feature affects datum plane orientation;
- Mathematical analysis of angularity, perpendicularity, and parallelism error;
- Improved visualizations of the complex, multi-dimensional design space.

Nomenclature

$\mathbf{B}$	build vector
h	layer thickness
L_d	length of datum
L_f	length of feature
$\mathbf{n_d}$	normal vector of datum feature
$\mathbf{n_f}$	normal vector of toleranced feature
δ	geometric deviation on a single layer
ϵ	error associated with a particular tolerance
θ	polar angle relative to feature
θ_d	polar angle relative to datum
ϕ	azimuthal angle relative to feature
ϕ_d	azimuthal angle relative to datum

2. Related work

Geometric dimensioning and tolerancing (GD&T) is the universal language used by designers to limit geometric deviation. Standards, such as ASME Y14.5 and ISO 1101, have been developed to establish universal definitions for different geometric tolerances [2,3]. This work will use definitions and concepts defined by ASME Y14.5-2009 to quantify geometric deviations

2212-8271 © 2018 The Authors. Published by Elsevier B.V.
Peer-review under responsibility of the Scientific Committee of the 15th CIRP Conference on Computer Aided Tolerancing - CIRP CAT 2018.
10.1016/j.procir.2018.03.315

on additively manufactured parts.

Many computer aided tolerancing systems have been developed to help designers assign design tolerances, based on functional constraints. Researchers have also studied tolerance allocation, optimizing the distribution of tolerances over several parts to minimize manufacturing cost, but previous work has focused on subtractive manufacturing processes. As summarized by Chase [4], a typical approach for allocating tolerances tries to optimize manufacturing cost based on theoretical manufacturing cost equations. A better understanding of the relationship between achievable geometric tolerances and manufacturing cost for AM would improve tolerance allocation. The layered, stair-step approximation typical of AM can be predicted mathematically from build direction and layer thickness, making it possible to explore trade-offs between geometric error and manufacturing cost, which are also a function of build direction.

The topic of analyzing geometric deviations for additively manufactured parts has long been of interest to researchers. Experimental work has been conducted to quantify the range of achievable tolerances for different AM processes [5,6]. Several previous studies focused on predicting and minimizing some geometric error metric, such as cusp height or volumetric deviation [7–10]. Some research has specifically analyzed the connection between AM errors and GD&T [8,11–14], allowing for integration with the tolerance allocation process. Arni and Gupta [12] and Paul and Anand [14] have performed mathematical analysis of geometric error associated with a particular tolerance (flatness and cylindricity, respectively). Mathematical analysis of error allows for quick computation of the error at many orientations, enabling real-time design feedback and fast iteration during tolerance allocation. However, in order for a design tool based on these approximations to be useful, it is necessary to evaluate a more complete set of tolerances. In this work, we do so for the three orientation tolerances, incorporating analysis of datums.

Visualization of build vector orientations that satisfy design or manufacturing constraints has been included in some previous work. Arni and Gupta sketched feasible orientations as regions on the surface of a unit sphere [12]. Rinaldi plotted feasible orientations using color to indicate the number of satisfied tolerances, plotting 2D contours of feasible regions with axes as x- and y-direction rotations [15]. Das et al. also used color to plot feasible regions on a unit sphere but only in increments of 10 degrees [13]. We expand on these approaches in the current work.

3. Mathematical Analysis

This work analyzes planar surfaces and planar datum features. Orientation tolerance zones for planar features are defined by two parallel planes within which the toleranced feature must be contained. The tolerance zone is oriented relative to one or more datums. Orientation error is defined here as the closest distance between two parallel planes, oriented by the datum, that contain every point on the toleranced surface. This error value can be compared to the tolerance value to determine if the as-manufactured feature is within tolerance.

We use a spherical coordinate system for our analysis, oriented to the toleranced feature face normal, $\mathbf{n_f}$. Following Arni and Gupta [12], the polar axis is aligned with $\mathbf{n_f}$; the polar angle, θ and azimuthal angle, ϕ, describe the orientation of the build vector, as seen in Fig. 1. The build vector, $\mathbf{B}$, is the direction normal to the build platform of the AM machine, orthogonal to the flat layers that are deposited.

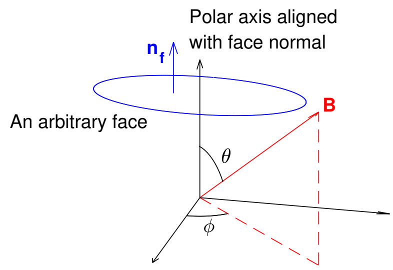

Fig. 1. Spherical coordinate system, adapted from [12]

For parallelism, the error for each feature face can be described using a single spherical coordinate system, oriented based on $\mathbf{n_f}$, because $\mathbf{n_f}$ is parallel to the datum face normal, $\mathbf{n_d}$. For angularity and perpendicularity, $\mathbf{n_f}$ and $\mathbf{n_d}$ are offset from each other by some angle; therefore, two local spherical coordinate systems are used. A second spherical coordinate system like that applied to the feature face (as shown in Fig. 1) is aligned to $\mathbf{n_d}$. The polar angle between $\mathbf{B}$ and $\mathbf{n_d}$, defined as θ_d, is shown in Fig. 2. For parallelism, $\theta_d = \theta$ because $\mathbf{n_d}$ and $\mathbf{n_f}$ are parallel.

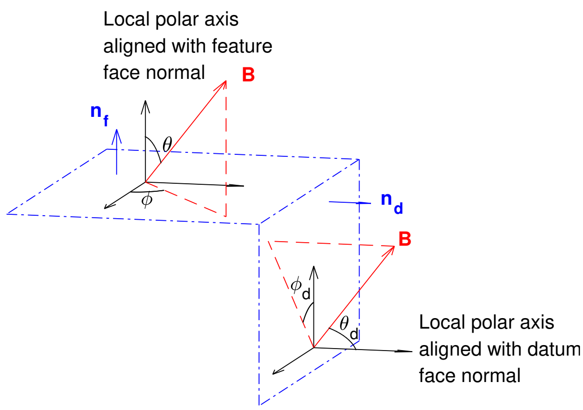

Fig. 2. Local coordinate systems for datum and some perpendicular feature

The orientation errors depend on the size of the part itself, as discussed in the next subsections. The size of the datum face and feature face, L_d and L_f respectively, can be calculated for $0 \leq \phi < 2\pi$ using the procedure that was described by Arni and Gupta [12] in the context of flatness error. Note that the datum face and feature face lengths are therefore functions of ϕ even though, for notational convenience, we will refer to them as L_f and L_d. This is done separately for both the toleranced feature and the datum feature. Because of the need for two coordinate systems for angularity and perpendicularity, we define two sets of mathematical models: one for parallelism; and one for angularity and perpendicularity.

In an effort to keep the model general for different AM processes, each individual layer is assumed to have a rectangular cross-section with a constant thickness. However, experimental studies have shown that individual layers are not perfect flat [16–18]. To incorporate geometric deviations of individual layers, we adopt the method of Arni and Gupta [12], and model a zone of finite thickness along the z- and xy- directions of each layer. The value of this deviation zone, δ_{xy} (parallel to $\mathbf{B}$) and δ_z (perpendicular to $\mathbf{B}$), can be experimentally determined for a particular process and machine. Because we model layer-level deviations as rectangular and because datum simulators used in orientation error measurement only contact high points of the datum feature faces, the layer-level deviation does not greatly affect datum plane orientation. Thus, the layer-level deviations are only modeled on the feature plane.

Support material, attached to downward facing faces, needs to be removed after printing and can also cause geometric deviations on individual layers. We introduce a support material geometric deviation, δ_s, which is added to δ_z if a feature face needs support. Whether a feature face needs support is determined by the angle between the build vector and the face normal vector. This cut off angle is process dependent, as is the value of the geometric deviation caused by support material removal.

3.1. Parallelism

We divide the equations that capture parallelism's error into three regimes. The error is equal to zero when the build vector is aligned or nearly aligned with $\mathbf{n_f}$ and $\mathbf{n_d}$. Both surfaces are approximated by one layer in this case, so the as-manufactured surfaces would both be parallel flat planes. The error in this regime, Regime 1, is equal to δ_z for parallelism, as shown in Fig. 3a.

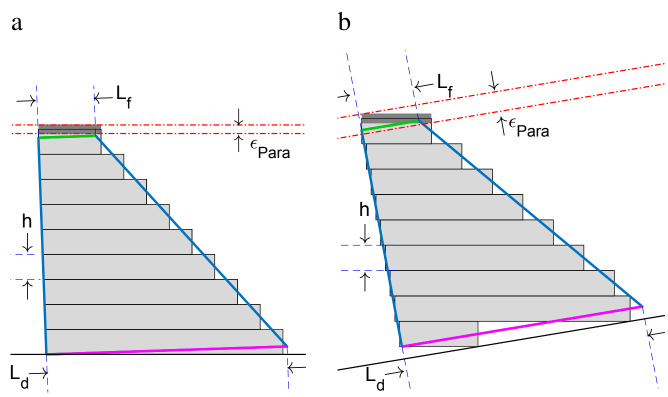

Fig. 3. Parallelism error, ϵ_{Para}. in (a) Regime 1 and (b) Regime 2 is shown as the distance between two red planes, oriented by the datum plane (black line). The outline of the theoretical perfect geometry is also shown, with the datum face highlighted in pink and the feature face displayed in green. δ_z is shown in dark gray.

The next regime, Regime 2, occurs when the datum face is approximated by at least two layers and the feature face is approximated by one layer. As the angle between $\mathbf{B}$ and $\mathbf{n_f}$ increases, the projection of the datum face on $\mathbf{B}$ will become large enough that the datum face is approximated by two layers. This transition occurs when the projection, $L_d \sin\theta$, is equal to $2h$ (where L_d is the length of the datum evaluated at a given ϕ). The polar angle at this transition, $\theta_{cr,1}$, can be calculated using Eq. 1. The error in this regime depends on the length of the feature, L_F, evaluated at a given ϕ, as seen in Fig. 3b.

Table 1. Parallelism error in various ranges, evaluated at a given value of ϕ

Regime	Range	ϵ_{Par} (length)
1	$0 \le \theta < \theta_{cr,1}$ $\pi - \theta_{cr,1} \le \theta < \pi$	δ_z
2	$\theta_{cr,1} \le \theta < \theta_{cr,2}$ $\pi - \theta_{cr,2} \le \theta < \pi - \theta_{cr,1}$	$L_f \sin\theta + \delta_z \lvert\cos\theta\rvert$
3	$\theta_{cr,2} \le \theta < \pi - \theta_{cr,2}$	$(h + \delta_z) \lvert\cos\theta\rvert + \delta_{xy} \sin\theta$

$$\begin{aligned} \theta_{cr,1}|_\phi &= \arcsin\left(\frac{2h}{L_d}\right) \\ \theta_{cr,2}|_\phi &= \arcsin\left(\frac{h}{L_f}\right) \end{aligned} \tag{1}$$

Equation 1 shows two distinct critical angles. This is due to the different roles of the datum feature and toleranced feature. For the datum feature, two layers were needed to establish a datum plane parallel to the theoretically perfect feature. For the approximated toleranced feature, the layered geometry doesn't define a plane. Rather, it must be contained by two planes whose orientation is determined by the datum plane. As long as the projection of the surface onto $\mathbf{B}$ is greater than h, the surface will be approximated by at least one plane, and the error follows the behavior of Regime 3. This regime switch occurs when θ is greater than $\theta_{cr,2}$, as defined in Eq. 1. If $\theta_{cr,2}$ is smaller than $\theta_{cr,1}$, Regime 1 dominates and Regime 2 won't be present. After this critical angle, the Regime 3 error is equal to $(h+\delta_z)\,|\cos\theta|+\delta_{xy}\sin\theta$. Regime 1 and 2 reoccur as θ approaches π. The errors and their corresponding ranges are shown in Table 1.

3.2. Angularity and perpendicularity

Angularity and perpendicularity follow a similar pattern to that of parallelism, but because of the offset between $\mathbf{n_d}$ and $\mathbf{n_f}$, there are now two separate coordinate systems to consider. Regime 1 occurs when $\mathbf{B}$ is aligned or nearly aligned with $\mathbf{n_d}$. The behavior in this regime is identical to that in Regime 1 for parallelism, where one layer is used to approximate the slanted datum surface, resulting in an offset between the datum plane and the perfect intended face. The offset between $\mathbf{n_d}$ and $\mathbf{n_f}$ results in a different error than that for parallelism in Regime 1. As shown in Fig. 4a, the angle misalignment causes an error approximately equal to $\left|L_f \sin\theta_d\right|$, while the layer approximation of the feature face results in an error equal to $(h + \delta_z)\,|\cos\theta| + \delta_{xy}\sin\theta$.

Regime 2 will occur when θ_d is greater than $\theta_{cr,1}$ but θ is less than $\theta_{cr,2}$. In this regime, $\mathbf{n_f}$ is nearly parallel to $\mathbf{B}$. The slanted feature face will be approximated by only one layer and the error is approximately equal to $\left|L_f \sin\theta\right| + \delta_z\,|\cos\theta|$, as shown in Fig. 4b. Both Regime 1 and 2 reoccur as θ approaches π. Regime 3 is the same as that for parallelism, where both features are approximated by several layers. The angularity or parallelism error as a function of the polar angle of the feature face, θ, and the polar angle of the datum face, θ_d, is summarized in Table 2.

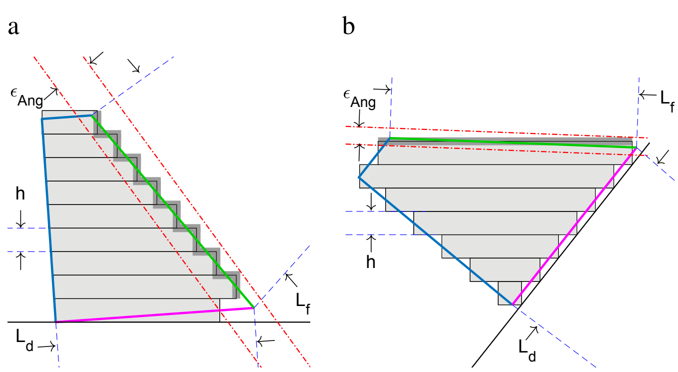

Fig. 4. ϵ_{Ang} in (a) Regime 1 and (b) Regime 2. δ_{xy} and δ_z are shown in dark gray.

Table 2. Angularity or perpendicularity error, evaluated at a given value of ϕ

Reg.	θ_d Range	θ Range	ϵ_{Par} or ϵ_{Ang}
1	$0 \leq \theta_d < \theta_{cr,1}$ $\theta_d \geq \pi - \theta_{cr,1}$	$0 \leq \theta \leq \pi$	$L_f \sin\theta_d + (h + \delta_z)\lvert\cos\theta\rvert$ $+\delta_{xy}\sin\theta$
2	$\theta_d \geq \theta_{cr,1}$	$0 \leq \theta < \theta_{cr,2}$ $\theta \geq \pi - \theta_{cr,2}$	$L_f \sin\theta + \delta_z \lvert\cos\theta\rvert$
3	$\theta_d \geq \theta_{cr,1}$	$\theta_{cr,2} \leq \theta < \pi - \theta_{cr,2}$	$(h + \delta_z)\lvert\cos\theta\rvert + \delta_{xy}\sin\theta$

3.3. Effect of slicing plane placement

Slicing of an STL file and processing of the sliced geometry into toolpaths is typically done through a software package (e.g. Cura or Slic3r). For a given orientation, the slicing process algorithm identifies the STL vertices closest to the build platform and takes a 2D slice of the geometry at some offset from this point (the offset is equal to $0.5h$ in Cura and Slic3r). The STL file is repeatedly sliced at $1.5h$, $2.5h$, and so on.

Because the transition between error regimes, discussed in Section 3.1 and 3.2, is defined by the θ at which the feature of interest begins to be approximated by one or two layers, the exact placement of slicing planes relative to the face can affect these transitions. This can be seen graphically in Fig. 5.

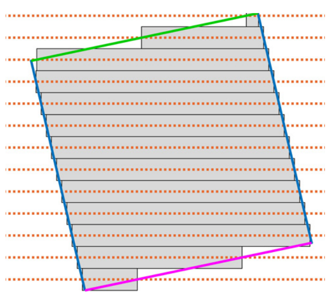

Fig. 5. Layered approximation of a rectangular shape with datum face shown in pink and feature face shown in green. Orange lines show slicing plane locations.

In Fig. 5, the datum and feature face have the same length, and are rotated by the same θ, so based on their projected length alone, it would be expected that both faces would be approximated by the same number of layers. However, the location of the slicing planes affects the number of layers approximating a face, so the feature face is approximated by three layers and the datum face is approximated by two layers. An exact calculation of the critical angles would need to consider the precise placement of the slicing planes relative the feature in question. The critical angles could occur at slightly lower values of θ than that predicted in Eq. 1. However, in practice, the difference between the theoretical critical angles and the actual angles for a particular slicing program is negligible because Regime 1 and 2 are very small for small layer thickness and large features.

4. Implementation

The system requires as input points on the edges of the feature face and datum face, normal vectors of the face and datum, the type of tolerance on each face, and the associated tolerance value. This geometry information can be manually found from the STL file or exported from a CAD system from the CAD model itself. The calculations performed for the example in this paper use geometry information directly from the CAD model and do not account for errors introduced by course STL resolution. For future work which will analyze non-planar geometry, the STL resolution will need to be considered for accurate error prediction.

The error for each tolerance is calculated separately. The build vector orientation is varied by 1 degree increments, from $0 \leq \phi \leq 2\pi$ and $0 \leq \theta \leq \pi$, and the error for each tolerance is calculated based on the equations summarized in Table 1 and 2. The computation time of this error is small as the only simple trigonometry functions are evaluated. The feasible regions are found by identifying build vector orientations where all specified tolerances are met. To provide additional information to the designer, the number of tolerances satisfied at all infeasible orientations is also given. The feasible orientations are plotted on a unit sphere, whose axes are aligned with the part axes.

5. Example application

To illustrate the system, the AM manufacturability of a jet engine bracket, using the geometry provided by GE for the GrabCAD additive manufacturing redesign challenge [19], was evaluated. We used the original geometry provided by GE (Fig. 6) but since the original design geometric tolerances were unspecified, all tolerances were inferred. The bottom face was chosen as a datum feature. Geometric tolerances were applied to three features, as shown in Fig. 6. We analyzed the achievable tolerances with layer thickness set to 0.15 mm, typical of a laser sintering process. The value of δ_{xy} was set to 0.12mm and δ_z was set to 0.05mm, based on experimental information [17]. δ_s was set to 0.05mm and was added to error calculations for build directions where the angle between $\mathbf{n_f}$ and $\mathbf{B}$ was greater than 135 degrees.

The error associated with each tolerance was calculated at 1 degree increments for all orientations of the build vector. Because the layer height is much smaller than the relevant part features, the critical angles are small; thus the error is dominated by the Regime 3 error for all three tolerances, as shown in Fig. 7. The error for each orientation is plotted on the unit sphere, similar to [12], but we use color to indicate the magnitude of error. The coordinate axes for the unit sphere are aligned with the coordinate axes of the part itself, shown in Fig. 6. This error map is similar to a visibility map [20], where the surface of the sphere is related to orientations of a vector, relative to a part.

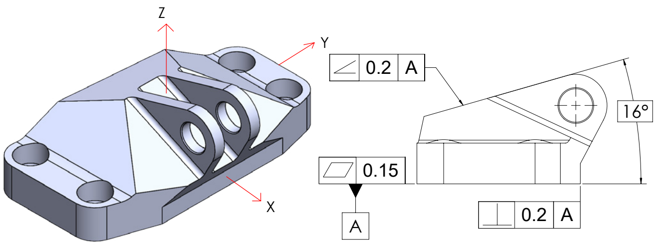

Fig. 6. GE redesign bracket [19] with tolerances added

To make the color scaling easy to understand and universally readable, we choose the Viridis colormap for its perceptually uniformity, its readability in grayscale, and interpretability by people with various forms of colorblindness [21].

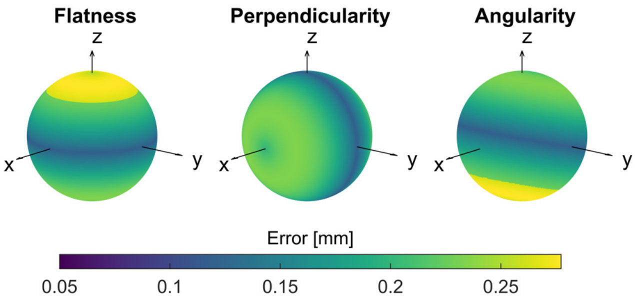

Fig. 7. Estimated error as a function of build vector orientation for example part

Angularity error is minimized if the build vector is exactly aligned with the feature normal, or if the build vector is orthogonal to the feature normal. This is also true for the perpendicularity error. The flatness error is oriented about the base plane. Flatness error is minimized if the build vector resides in the xy plane or if it is parallel to the z-axis. The increased error due to support material removal on the feature face is visible at the bottom of the angularity error plot and the top of the flatness error plot.

Because the critical angles are small, the regions associated with Regime 1 and 2 are small. An enlarged view of the $+x$ face of the error sphere is shown in Fig. 8a. If the build vector is perfectly aligned with the x-axis, $\mathbf{B} =< 1, 0, 0 >$, the perpendicularity error is equal to δ_z, and the face is approximated by one flat plane. If there is more than a slight misalignment, the error is larger in magnitude because the error regime switches to Regime 3. If the ratio of layer height to face length was larger, the critical angles would be larger and the influence of Regime 1 and 2 would be more apparent, as shown in Fig. 8b, which shows the same result but with a layer height of 1.0mm.

Fig. 9 shows a unit sphere containing all possible orientations of the build vector. Green regions denote orientations of the build vector that result in all specified tolerances on the example part being satisfied. If $\mathbf{B}$ was aligned with the positive x- or y-axis of the example part (see coordinate system shown in Fig. 6), then all three specified tolerances would be satisfied, which would not be the case with the original build orientation (positive z-axis).

Region A contains only a small range of orientations, which is why it is displayed as a small dot rather than a large area.

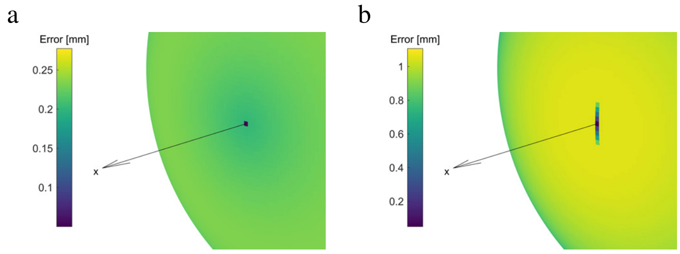

Fig. 8. Perpendicularity error when build vector is nearly aligned with x-axis for (a) h = 0.15mm; (b) h = 1mm

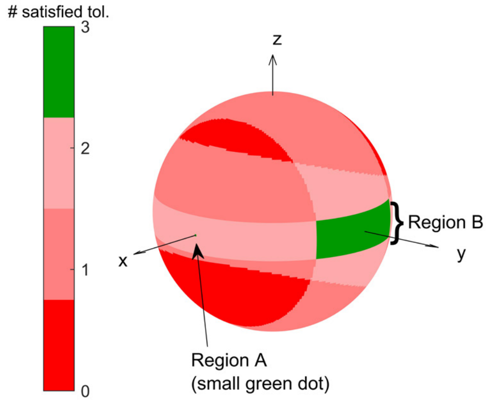

Fig. 9. Feasibility regions for example part

Region B is much larger, giving a wide range of feasible orientations.

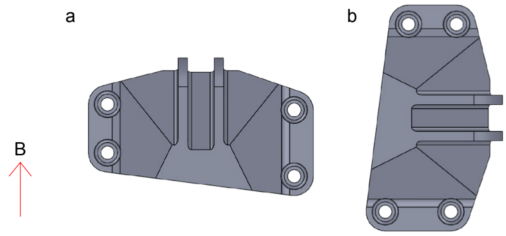

Fig. 10. Orientation of object at (a) $\mathbf{B} =< 1, 0, 0 >$ (b) $\mathbf{B} =< 0, 1, 0 >$

6. Discussion

The feasible regions help to identify orientations where all tolerances are met but do not convey information about the specific magnitude of the errors in the region. Considering the estimated errors for all three tolerances shown in Fig. 7, it can be seen that if the build vector is aligned with the y-axis, the errors for all three tolerances are equal to 0.12mm. Within the range of feasible orientations, this specific orientation results in low geometric error for all three tolerances, and should be chosen as the final build orientation if that is the only objective. This level of error is of the same order of magnitude as geometric deviations reported in other work [6]. In future work, we intend to validate our model by manufacturing and inspecting parts and comparing these measurements to the model predictions.

The example part illustrates how dominant Regime 3 is for all orientations. The orientations corresponding to Regime 1 and 2 correspond to a range of approximately 1 degree and are only visible upon close inspection of the error plots and feasible region plots. This is due to the large size of the bracket, compared to the layer thickness of 0.15mm. As h decreases, the range of Regime 1 and Regime 2 become smaller; the effect of the slicing plane placement influences a smaller portion of the overall error function. Regime 1 and 2 error is most important for large ratios of h to L_f and L_d, which correspond to larger values of $\theta_{cr,1}$ and $\theta_{cr,2}$. The effect of slicing plane placement will also become increasingly important for small features and datums with large ratios of h to L_f and L_d.

The mathematical formulas of error allow for real-time computation of the feasible regions. The calculation of the error for 64,800 orientations, identification of orientations that needed support, and identification of feasible regions for the example problem shown here took 0.933 seconds to run in a MATLAB implementation. An advantage of the mathematical basis of our approach is speed but it is difficult to model the effect of machine inaccuracy or thermal deviations. In future work, we hope to develop more probabilistic estimates which include some of these effects, similar to the work of Moroni et al. [8].

The visualizations shown here use color to represent magnitude of error or varying shades of red and green to indicate number of achieved tolerances. It is hoped that this visualization, especially due to the perceptual uniformity of the error colormap, will enable designers to quickly evaluate potential build vector orientations.

7. Conclusion

This system is able to quickly calculate orientation and flatness errors for multiple features and can identify build directions that result in the satisfaction of all tolerances. Mathematical analysis of the angularity, perpendicularity, and parallelism error enables efficient prediction of error due to the stair-stepped approximation characteristic of AM. The system is material-general and can be utilized for any layer-based process with fixed layer thickness.

This type of design tool can help bridge the gap between designers and manufacturers, allowing designers to understand and optimize for manufacturing constraints before their parts are actually manufactured. A tool that predicts tolerances are mutually achievable for a part can improve the tolerance allocation process. Further, this tool can elucidate relationships between layer thickness, orientation, and geometric deviation errors.

This error prediction approach could be used as the basis of a manufacturing trade-off system that could improve tolerance allocation and other design decisions influence by manufacturing cost. Other process parameters that are affected by build orientation, such as print time and material usage, could be added to this system to help estimate manufacturing cost. Such a system could be helpful for designers to directly explore the increased cost of tight tolerances. Further analysis of different types of visualizations is needed to help designers efficiently explore the complicated design space. The authors also plan to add the evaluation of other types of geometric tolerances to the system's capabilities.

Acknowledgments

This material is based upon work supported by the National Science Foundation Graduate Research Fellowship Program under Grant No. 1106400. Any opinions, findings, and conclusions or recommendations expressed in this material are those of the authors and do not necessarily reflect the views of the National Science Foundation.

References

[1] I. Gibson, D. Rosen, B. Stucker, Additive Manufacturing Technologies, 2nd Edition, Springer, 2015.
[2] Dimensioning and Tolerancing ASME Y14.5 (2009).
[3] ISO 1101:2017 Geometrical product specifications (GPS) - tolerances of form, orientation, location and run-out. (2017).
[4] K. Chase, Tolerance allocation methods for designers, Tech. Rep. 99-6, Brigham Young University (1999).
[5] S. Mahmood, D. Talamona, L. K. Goh, A. J. Qureshi, Fast Deviation Simulation for Fused Deposition Modeling Process, Procedia CIRP 43 (2016) 327–332. doi:10.1016/j.procir.2016.02.004.
[6] T. Lieneke, G. A. O. Adam, S. Leuders, F. Knoop, S. Josupeit, P. Delfs, N. Funke, D. Zimmer, Systematical determination of tolerances for additive manufacturing by measuring linear dimensions, Solid Free. Fabr. Symp. (2015) 371–384.
[7] G. Moroni, S. Petrò, W. Polini, Geometrical product specification and verification in additive manufacturing, CIRP Ann. - Manuf. Technol. 66 (1) (2017) 157–160. doi:10.1016/j.cirp.2017.04.043.
[8] G. Moroni, W. P. Syam, S. Petrò, Towards early estimation of part accuracy in additive manufacturing, Procedia CIRP 21 (2014) 300–305. doi:10.1016/j.procir.2014.03.194.
[9] D. Ahn, H. Kim, S. Lee, Surface roughness prediction using measured data and interpolation in layered manufacturing, J. Mater. Process. Technol. 209 (2) (2009) 664–671. doi:10.1016/j.jmatprotec.2008.02.050.
[10] K. Thrimurthulu, P. M. Pandey, N. V. Reddy, N. Venkata Reddy, Optimum part deposition orientation in fused deposition modeling, Int. J. Mach. Tools Manuf. 44 (6) (2004) 585–594. doi:10.1016/j.ijmachtools.2003.12.004.
[11] A. P. West, S. P. Sambu, D. W. Rosen, Process planning method for improving build performance in stereolithography, Comput. Des. 33 (1) (2001) 65–79. doi:10.1016/S0010-4485(00)00064-6.
[12] R. Arni, S. K. Gupta, Manufacturability Analysis of Flatness Tolerances in Solid Freeform Fabrication, J. Mech. Des. 123 (1) (2001) 148–156. doi:10.1115/1.1326439.
[13] P. Das, R. Chandran, R. Samant, S. Anand, Optimum Part Build Orientation in Additive Manufacturing for Minimizing Part Errors and Support Structures, Procedia Manuf. 1 (2015) 343–354. doi:10.1016/j.promfg.2015.09.041.
[14] R. Paul, S. Anand, Optimal part orientation in Rapid Manufacturing process for achieving geometric tolerances, J. Manuf. Syst. 30 (4) (2011) 214–222. doi:10.1016/j.jmsy.2011.07.010.
[15] A. Rinaldi, Design methodology for geometric dimensioning and tolerancing in additively manufactured parts, Masters thesis, ETH Zurich (2017).
[16] A. Boschetto, V. Giordano, F. Veniali, Modelling micro geometrical profiles in fused deposition process, Int. J. Adv. Manuf. Technol. 61 (9-12) (2012) 945–956. doi:10.1007/s00170-011-3744-1.
[17] A. Boschetto, L. Bottini, F. Veniali, Roughness modeling of AlSi10Mg parts fabricated by selective laser melting, J. Mater. Process. Technol. 241 (2017) 154–163. doi:10.1016/j.jmatprotec.2016.11.013.
[18] P. E. Reeves, R. C. Cobb, Rapid Prototyping Journal Reducing the surface deviation of stereolithography using in-process techniques, Rapid Prototyp. J. 3 (4) (1997) 20–31. doi:10.1108/13552549710169255.
[19] GE jet engine bracket challenge (2013). URL `https://grabcad.com/challenges/ge-jet-engine-bracket-challenge`
[20] T. C. Woo, Visibility maps and spherical algorithms, Comput. Des. 26 (1) (1994) 6–16. doi:10.1016/0010-4485(94)90003-5.
[21] S. van der Walt, N. Smith, mpl colormaps (2015). URL `http://bids.github.io/colormap/`